

CHEMICAL ABUNDANCES FOR A-AND F-TYPE SUPERGIANT STARS

R. E. Molina and H. Rivera

Laboratorio de Investigación en Física Aplicada y Computacional, Universidad Nacional Experimental del Táchira, Venezuela

Received May 9 2016; accepted July 11 2016

RESUMEN

Hemos efectuado un análisis detallado de las abundancias químicas de cuatro objetos supergigantes HD 45674, HD 180028, HD 194951 y HD 224893, usando espectros de alta resolución ($R \approx 42,000$) tomados de la librería ELODIE. Se presentan los primeros resultados de las abundancias para HD 45674 y HD 224893, y se reafirman las abundancias para HD 180028 y HD 194951 calculadas por Luck. Los elementos alfa nos indican que todos los objetos estudiados pertenecen a la población del disco galáctico. Sus abundancias y su localización en el diagrama Hertzsprung-Russell parecen indicarnos que HD 45675, HD 194951 y HD 224893 evolutivamente se encuentran en la fase posterior al primer dragado (post-1DUP) y se mueven en la región del lazo rojo-azul (*red-blue loop*). HD 180028 muestra abundancias típicas de la Población I pero su estado evolutivo no puede ser definido satisfactoriamente.

ABSTRACT

We present the stellar parameters and elemental abundances of a set of A–F-type supergiant stars HD 45674, HD 180028, HD 194951 and HD 224893 using high resolution ($R \approx 42,000$) spectra taken from ELODIE library. We present the first results of the abundance analysis for HD 45674 and HD 224893. We reaffirm the abundances for HD 180028 and HD 194951 studied previously by Luck. Alpha-elements indicate that the objects belong to the thin disc population. Their abundances and their location on the Hertzsprung-Russell diagram seem to indicate that HD 45675, HD 194951 and HD 224893 are in the post-first dredge-up (post-1DUP) phase, and that they are moving in the red-blue loop region. HD 180028, on the contrary, shows typical abundances of Population I, but its evolutionary status cannot be satisfactorily defined.

Key Words: stars: abundances — stars: atmospheres — stars: evolution — supergiants

1. INTRODUCTION

The process of chemical evolution in the Galaxy can be understood from the study of its massive stars. These objects in their rapid evolution undergo changes through the process of nucleosynthesis and return their chemical elements to the interstellar medium by stellar winds and supernova events. The existence of massive young objects in the galactic plane is not surprising, since it is an area of star formation. These objects are visually luminous in galaxies and thus are suitable candidates for studies of stellar and chemical evolution (Luck et al. 1998;

Smiljanic et al. 2006; Venn et al. 2000, 2001, 2003; Kaufer et al. 2004).

Some of these massive objects have been classified as supergiant stars with masses between 5 to $20 M_{\odot}$, and A-and-F spectral types, which are moderately evolved. The chemical abundances of the light elements CNO have been crucial to discriminate their evolutionary states (Lyubimkov et al. 2011, Venn 1995a,1995b and references therein). When H is exhausted in massive stars the post-He core burning phase can be affected in several ways.

Stellar evolutionary models constructed for solar metallicities predict that massive supergiants ($M \geq 10 M_{\odot}$) are in the phase of helium core burning (Schaller et al. 1992; Stothers & Chin 1991). These objects have already left the main sequence and begun the ignition of He in the blue supergiant region, but thermal instabilities cause in them a rapid expansion towards a red supergiant phase. In this phase, the A–F supergiants are able to resume thermal and radiative equilibrium through convection in the outer layers and shows an altered CNO abundance due to the first dredge-up (1DUP) event.

On the other hand, less massive A–F supergiants ($M < 10 M_{\odot}$) have also initiated the He-core burning without visiting the red giant branch, they develop a fully convective intermediate zone, the envelope is able to establish thermal equilibrium and the stars stay in the blue supergiant phase. Under these conditions CNO abundances remain unchanged (Stothers & Chin 1976; 1991).

However, another scenario is possible for objects with intermediate masses ($3 < M < 9 M_{\odot}$) and it is called the blue loop. In this stage the star has eventually developed a convective envelope and is rising up the Hayashi line in the HRD. These objects have already reached the red supergiant stage but eventually evolve back into a blue supergiant phase (Walmswell et al. 2015). During the red supergiant phase, the convective zone mixes materials of the H-burning shell, which are subsequently released to the surface by the 1DUP event, causing changes in the observed CNO abundance patterns. The amount CNO-processed material in such objects allows us to discriminate between different types of supergiants.

The main goal of this work is a detailed study of chemical abundances for a set of four low-latitude A–F supergiants: HD 45674, HD 180028, HD 194951 and HD 224893, under the assumption of LTE, as well as the determination of their atmospheric parameters from excitation and ionization equilibrium. For this purpose we employ high-resolution spectroscopy and a set of atmospheric models constructed with plane-parallel geometry, hydrostatic equilibrium, local thermodynamic equilibrium (LTE) and the ODFNEW opacity distribution (Castelli & Kurucz 2004). It is expected that the abundances derived correspond to the typical abundances observed for supergiant stars in the galactic disc.

This paper is organized as follows: In § 2 we describe the sample selection. In § 3 we present how the atmospheric parameters were estimated. We determine the chemical abundances for the three stars

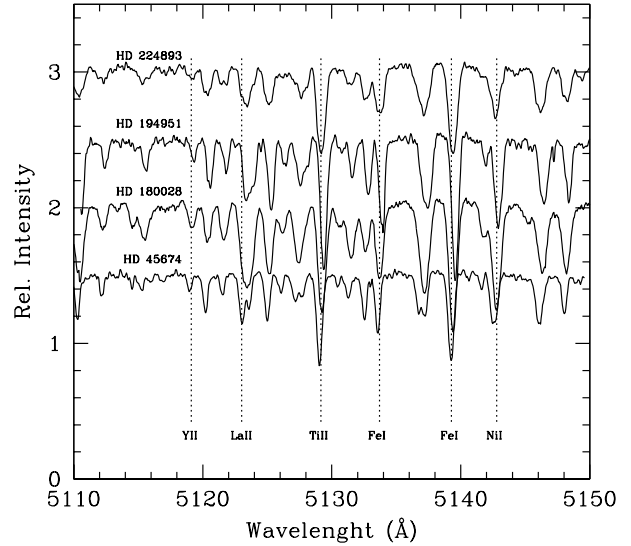


Fig. 1. Representative spectra of the sample stars HD 45674, HD 180028, HD 194951 and HD 224893. The locations of lines of certain important elements have been indicated by dashed lines. This stars are arranged in decreasing order the HD number.

in § 4. An individual analysis of abundances for each stars is presented in § 5. § 6 is dedicated to discuss our results, and finally, § 7 gives the conclusions of the paper.

2. OBSERVATIONS

2.1. Sample Selection

The stars for this analysis (HD 45674, HD 180028, HD 194951 and HD 224893) were selected because they are luminous objects of Classes I and II located in the galactic plane. The derived abundances are compared with the mean abundances obtained for a sample of G–K young supergiants of Population I taken from Luck (1977; 1978).

The stellar spectra taken for HD 45674, HD 180028, HD 194951 and HD 224893 are taken from the library ELODIE¹ originally published by Moultaqa et al. (2001) and updated in its version 3.1 by Prugniel et al. (2007). The spectra were observed on July 06, 1999; on July 26, 2003; on December 18, 1999 and on July 07, 1999 respectively by means of the echelle spectrograph ELODIE placed in the 1.93m telescope located in the Haute-Provence Observatory (OHP). They cover the spectral region between 4000 and 6800 Å, and have a resolving power of $R \approx 42,000$. The signal-to-noise ratio (S/N) for

¹<http://atlas.obs-hp.fr/elodie/>

TABLE 1
BASIC PARAMETERS FOR THE SAMPLE

HD	SpT	α (h m s)	δ ($^{\circ}$ ' ")	V (mag)	B (mag)	l ($^{\circ}$)	b ($^{\circ}$)	V_r (km s^{-1})	π (mas)	$E(B-V)$ (mag)	$v \sin i$ (km s^{-1})
45674	F1Ia	06 28 47	-00 34 20	6.56	7.30	210.85	-05.30	+18.4 \pm 0.9	1.31 \pm 0.51	0.382	...
180028	F6Ib	19 14 44	+06 02 54	6.96	7.73	040.97	-02.39	-5.1 \pm 0.7	-0.32 \pm 0.51	0.346	23.3
194951	F1II	20 27 07	+34 19 44	6.41	6.84	073.86	-02.34	-13.5 \pm 2.0	1.00 \pm 0.41	0.230	20
224893	A8II	00 01 37	+61 13 22	5.57	5.94	116.97	-01.07	-23.2 \pm 2.0	1.06 \pm 0.27	0.244	40

HD 45674, HD 180028, HD 194951 and HD 224893 is reported to be 83, 175, 82 and 145 respectively. This S/N per pixel has been derived for all spectra in the library at 5550 Å.

HD 45674, HD 180028 and HD 194951 are objects labeled as IRAS point sources, (IRAS 06262-0032, IRAS 19122+0557 and IRAS 20252+3410 respectively), although none of them display reliable infrared excesses since their IRAS fluxes are of low quality ($Q=1$) at 25, 60 and 100 microns. A review of the spectral energy distributions (SED) from the available photometry contained in the VisIER database also indicates that flux data from other sources like WISE and AKARI for these three objects do not indicate infrared excesses. Likewise, HD 224893 does not show evidence of dust around the central star. This last object was identified by Bidelman (1993) as a possible candidate to a post-AGB or normal A- and F-type supergiant star.

Figure 1 shows a representative range of 50 Å of the spectrum for the stars HD 45674, HD 180028, HD 194951 and HD 224893. The vertical dotted lines indicate the position of some absorption lines of elements such as Y II, La II, Ti II, Fe I y Ni I. The basic parameters for the total sample are shown in Table 1. This table contains the HD number, the equatorial coordinates, the apparent V and B magnitude, the galactic coordinates, the radial velocity, the parallax, the color excess and the velocity of rotation. These values were taken from the SIMBAD astronomical database.²

3. ATMOSPHERIC PARAMETERS

In order to obtain the atmospheric parameters accurate measurements of the equivalent widths (E_w) of the Fe lines are necessary as well as measurements of atomic data ($\log g$ and χ (eV)). The atomic data for the Fe I and Fe II lines were taken from Führ & Wiese (2006) and Meléndez & Barbuy (2009). The E_w values were restricted to a range from 10 to 200 mÅ, and only non-blended lines were measured. To measure the E_w we used the task

²<http://simbad.u-strasbg.fr/simbad/>

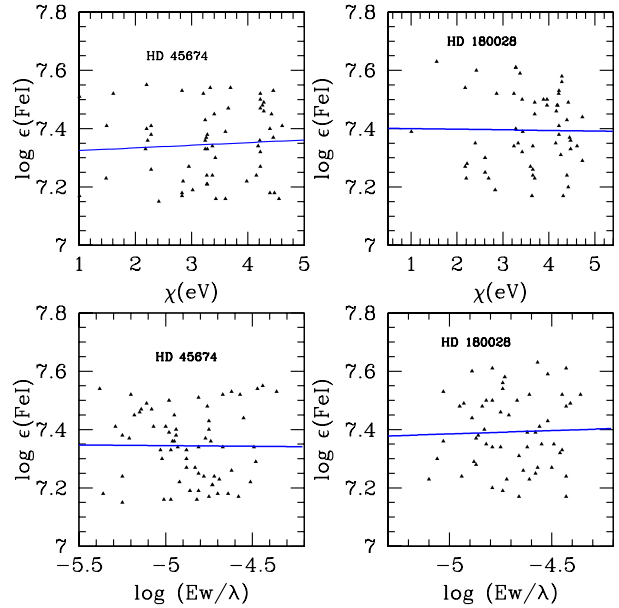


Fig. 2. Independence of Fe I abundances from the low potential excitation and reduced equivalent widths in HD 45674 and HD 180028.

SPLIT of the IRAF software with a Gaussian fit to the observed line profiles. The error in the measurements of E_w is about 8-10%.

The stellar atmospheric models for the abundance determinations were selected from the collection of Castelli and Kurucz (2003). These models have been constructed with a plane-parallel geometry, hydrostatic equilibrium, local thermodynamic equilibrium (LTE) and the ODFNEW opacity distribution.

We used the updated version (2010) of the MOOG code (Snedden 1973) for the determination of the atmospheric parameters. This code has been developed under ETL assumptions. Based on a trial and error test, we selected the model that best fitted the photosphere of stars. With the best model, the effective temperature was determined under the assumption of excitation equilibrium, i.e., by requiring the derived iron abundances to be independent of the low excitation potential. The surface gravity was de-

TABLE 2
ATMOSPHERIC PARAMETERS DERIVED IN THIS WORK AND THOSE OBTAINED
FROM THE LITERATURE

HD	T_{eff} (K)	$\log g$	ξ_t (km s^{-1})	[Fe/H]	Ref.
45674	7346	1.95		+0.18	Prugniel & Soubiran (2001)
	7630	2.05		+0.16	Wu et al. (2011)
	7488±200	2.00±0.07		+0.17±0.01	Mean Value
	7500	2.0	4.0	+0.16	This Work (adopted)
180028	6280	1.72	4.6	-0.03	Gray et al. (2001b)
	6531	1.54		-0.01	Prugniel & Soubiran (2001)
	6050	1.3	3.0		Andrievsky et al. (2002)
	6287	1.65		+0.14	Wu et al. (2011)
	6307	1.9	4.0	+0.10	Kovtyukh et al. (2012)
	6488	2.32	4.08	+0.26	Luck (2014)
	6502	2.46	4.11	+0.39	Luck (2014)
	6349±171	1.84±0.42	3.96±0.59	+0.14±0.16	Mean Value
	6400	2.1	4.8	-0.06	This Work (adopted)
194951	6950	2.02		-0.09	Gray et al. (2001b)
	6350	1.0	2.8		Andrievsky et al. (2002)
	7392				Kovtyukh et al. (2007)
	7268				Hohle et al. (2010)
	6760	1.92		-0.13	Lyubimkov et al. (2011)
	7019	2.22	3.93	+0.08	Luck (2014)
	6977	2.21	3.87	+0.11	Luck (2014)
	6959±341	1.87±0.50	3.53±0.64	-0.01±0.12	Mean Value
7000	1.8	4.7	-0.15	This Work (adopted)	
224893	7340	1.96	3.9	-0.24	Gray et al. (2001b)
	7500	2.0	4.5	-0.26	This Work (adopted)

rived by requiring that the Fe I abundances be similar to those obtained for the Fe II. To confirm the value of the gravity, the equilibrium condition can be extended to other elements with two ionization states like Ca, Ti, Cr, Ni. Finally the microturbulence velocity was determined by requiring that the abundances of Fe I be independent of the reduced equivalent widths ($\log Ew/\lambda$). Figure 2 shows that the abundances of Fe I are independent of the low excitation potential and of the reduced equivalent widths for HD 45674 and HD 180028.

Table 2 lists the atmospheric parameters estimated by different authors from photometric and spectroscopic techniques and also the atmospheric parameters adopted for this work. For objects with more than one measure a mean value for their atmospheric parameters was estimated. We note that our adopted atmospheric parameters match satisfactorily these mean values.

3.1. Uncertainty in the Abundances

We calculated the effects on the chemical abundances of errors in the measured equivalent widths (8–10%), the defined model of atmospheric parameters (+250 K in T_{eff} , +0.5 in $\log g$ and +0.5 km s^{-1} in ξ_t), and the atomic data ($\log gf$ and χ (eV)). Errors due to equivalent widths are random because they depend on several factors, such as the position of the continuum, the signal to noise ratio (S/N) and the spectral type of the star.

In contrast, errors due to the atmospheric parameters and atomic data are systematic and depend on the quality with which they were derived. In short, the error in the gf -values can vary from element to element. For example, experimental values of high accuracy for Fe I and Fe II between 3% to 10% are available for a large fraction of the lines. For other Fe-peak elements, errors in their gf -values

TABLE 3

SENSITIVITY OF ABUNDANCES TO THE UNCERTAINTIES IN THE MODEL PARAMETERS FOR TWO RANGES OF TEMPERATURE SPANNING OUR SAMPLE STARS

Species	HD 45674 (7500 K)					HD 180028 (6400 K)				
	ΔT_{eff} +250 K	$\Delta \log g$ +0.5	$\Delta \xi_t$ +0.5	ΔE_w +10%	σ_{tot}	ΔT_{eff} +250 K	$\Delta \log g$ +0.5	$\Delta \xi_t$ +0.5	ΔE_w +10%	σ_{tot}
C I	-0.14	0.00	+0.01	-0.01	0.14	+0.07	-0.11	-0.01	0.00	0.13
N I	-0.02	-0.06	0.00	-0.01	0.06
O I	+0.02	-0.08	+0.01	-0.01	0.08	+0.10	-0.05	0.00	...	0.11
Na I	-0.20	+0.08	+0.01	-0.01	0.22	-0.03	-0.03	+0.05	-0.01	0.07
Mg I	-0.22	+0.08	+0.08	-0.01	0.25	-0.14	-0.04	+0.04	0.00	0.15
Si I	-0.03	-0.03	+0.01	0.00	0.04
Si II	+0.02	-0.08	+0.16	-0.02	0.18	+0.13	-0.15	+0.07	-0.01	0.21
S I	-0.17	+0.04	+0.02	-0.01	0.18	+0.04	-0.11	+0.02	-0.01	0.12
Ca I	-0.27	+0.10	+0.05	-0.01	0.29	-0.07	-0.02	+0.04	-0.01	0.08
Ca II	-0.07	-0.04	+0.03	0.00	0.09
Sc II	-0.15	-0.12	+0.07	-0.01	0.20	-0.04	-0.16	+0.03	-0.01	0.17
Ti I	-0.28	+0.05	0.00	-0.02	0.29	-0.14	-0.04	+0.01	-0.01	0.15
Ti II	-0.15	-0.13	+0.08	-0.02	0.21	-0.03	-0.16	+0.04	-0.01	0.17
V II	-0.13	-0.12	+0.02	-0.01	0.18
Cr I	-0.27	+0.06	+0.03	-0.01	0.28	-0.12	-0.04	+0.03	-0.01	0.13
Cr II	-0.10	-0.12	+0.05	-0.01	0.16	+0.03	-0.16	+0.06	-0.02	0.17
Mn I	-0.24	+0.07	+0.02	-0.01	0.25	-0.08	-0.04	+0.04	-0.01	0.10
Fe I	-0.24	+0.07	+0.03	-0.01	0.25	-0.08	-0.04	+0.04	-0.01	0.10
Fe II	-0.10	-0.12	+0.04	-0.01	0.16	+0.02	-0.15	+0.05	-0.01	0.16
Ni I	-0.22	+0.08	+0.01	0.00	0.23	-0.08	-0.04	+0.02	-0.01	0.09
Cu I	-0.13	-0.04	+0.01	-0.01	0.14
Zn I	-0.24	+0.07	+0.01	0.00	0.25	-0.08	-0.05	+0.02	-0.01	0.10
Y II	-0.19	-0.11	+0.03	-0.01	0.22	-0.04	-0.16	+0.02	0.00	0.17
Zr II	-0.17	-0.13	+0.05	-0.02	0.22	-0.03	-0.16	+0.01	0.00	0.16
Ba II	-0.30	0.00	+0.05	-0.01	0.30	-0.10	-0.10	+0.07	...	0.15
La II	-0.08	-0.16	+0.06	-0.02	0.19
Ce II	-0.24	-0.08	+0.01	-0.01	0.25	-0.08	-0.15	+0.01	0.00	0.17
Nd II	-0.28	-0.05	0.00	0.00	0.28	-0.11	-0.15	+0.01	0.00	0.19
Eu II	-0.10	-0.18	0.00	...	0.20

may range from 10 to 25%. For neutron- capture elements the accuracy is in the 10 to 50% range. The sensitivity of the derived abundances to changes in the model atmosphere parameters is displayed in Table 3.

HD 45674 and HD 194951 have the same temperature, i.e., 7500 K. For these stars the spectra are much cleaner and the temperature is not large enough for the lines to develop strong wings making line strengths inaccurate. We can see that a variation in effective temperature of 250 K generates a

greater uncertainty in all lines, particularly in neutral lines except C, N, O and ionized lines like Ba, Ce and Nd. On the contrary, we did not observe significant changes in the uncertainties due to changes in $\log g$ by 0.5, ξ_t by 0.5 km s^{-1} and E_w by 10 per cent. However, at a lower temperature (6400 K) the line strengths shows sensitivity only to changes both in T_{eff} by 250 K, and in $\log g$ by 0.5.

The total error σ_{tot} for each element is given by the square root of the quadratic sum of the random and systematic errors.

4. DETERMINATION OF THE ABUNDANCES

For the determination of chemical abundances we used the equivalent widths of 176, 116, 184 and 73 absorption lines identified in HD 45674, HD 180028, HD 194951 and HD 224893, respectively. We use the task ABFIND of the MOOG code (Snedden 1973). We employ the atmospheric models adopted in Table 2. The sources of the gf -values for different elements are those given by Sumangala Rao, Giridhar and Lambert (2012) (see Table 4 for further details).

Sumangala Rao, Giridhar and Lambert (2012) also studied the systematic differences caused when they used different sources for gf -values. The authors employed the solar spectrum from the Solar Flux Atlas (Kurucz et al. 1984) and found very few differences in the solar values for most of the elements, i.e., between 0.04 to 0.09 dex.

The chemical abundances derived for HD 45674, HD 180028, HD 194951 and HD 224893 can be seen in Table 4. This table contains the chemical species present in the photosphere, the solar photospheric abundances as given by Asplund et al. (2005), as well as those calculated for each star and their uncertainty, the abundances relative to hydrogen, the number of identified lines and the abundances relative to iron. The abundances of the elements in Table 4 are in a logarithmic scale with respect to hydrogen, namely: $\log \epsilon(X) = \log [N(X)/N(H)] + 12.0$. The abundances of the elements relative to hydrogen and iron are expressed as $[X/H] = \log \epsilon(X)_{\text{star}} - \log \epsilon(X)_{\text{sun}}$ and $[X/Fe] = [X/H] - [Fe/H]$ respectively.

5. DISCUSSION OF THE INDIVIDUAL ABUNDANCES

5.1. HD 45674

The star HD 45674 has been classified as F1Ia. Bidelman (1993) includes this object as a possible candidate to a post-AGB or an A-and-F normal supergiant star. The atmospheric parameters were obtained from ionization equilibrium between the lines of Fe I and Fe II with values of $T_{\text{eff}} = 7500$ K, $\log g = 2.0$, $\chi_t = 4.0$ and $[Fe/H] = +0.16$ dex respectively. The surface gravity for HD 45674 was confirmed from the equilibrium ionization of other elements such as Ca, Ti, Cr, from which $\Delta = [X_{\text{II}}/H] - [X_{\text{I}}/H]$ is 0.08, -0.02 and -0.05 respectively. A compilation of the atmospheric parameters obtained by different authors is shown in Table 2.

With respect to the abundances of the light elements CNO, the carbon abundance was obtained from two lines (4769 Å and 5380 Å) their values being $[C/H] = -0.20$ and $[C/Fe] = -0.36$. Venn (1995b)

predicts a non-LTE correction of -0.25 in the C abundance for the supergiant HD 36673 (F0Ib) with an effective temperature of 7400 K. HD 45674 has an effective temperature of 7500 K; therefore no non-LTE correction was necessary. A value of -0.25 dex led to an abundance of $[C/Fe] = -0.69$.

The N abundance for HD 45674 showed a moderate enrichment ($[N/Fe] = +0.68$). In fact, this abundance was obtained from the $\lambda 4151.4$ Å line with an Ew of 10.1 mÅ. A non-LTE correction of -0.28 was derived by Venn (1995b) in the near IR region at 7400 K for this star, which is of A9II type. The non-LTE correction for N I by Luck & Lambert (1985) indicated that at a temperature of 7500 K, an equivalent width of ≈ 10 mÅ and $\log g = 2.0$, the non-LTE correction is almost zero (see Figure 8). By contrast, for the blue region Przybilla & Butler (2001) found a non-LTE correction of -0.11 dex for N I ($\lambda 3830$ Å) at a temperature of 9600 K and with a negatively increasing value toward the IR lines. Taking into consideration the above we can argue that the non-LTE correction should be small for this line.

We adopted a value of ≈ -0.08 dex for our line in the blue region. Our non-LTE values are $[N/H] = +0.60$ dex and $[N/Fe] = +0.36$ dex respectively. The observed deficiency of C and the moderate enhancement of N involves a conversion of initial carbon into N through the CN-cycle and products of the 1DUP being brought to the surface.

The O abundance is near solar ($[O/Fe] = +0.03$), and is obtained from the $\lambda 6156.0$ Å and $\lambda 6156.8$ Å lines. At this temperature a non-LTE correction of about -0.15 (taken from Takeda & Takada-Hidai 1998) would lead to abundances of $[O/H] = -0.12$ and $[O/Fe] = -0.36$ respectively. The C/O ratio of 0.32 indicates that HD 45674 is O-rich.

Iron-peak elements (Sc, V, Cr, Ni) show $[X/Fe]$ abundances very similar to solar, and ranges from -0.22 to $+0.18$ dex. The $[\alpha/Fe]$ ratio $\approx +0.10 \pm 0.16$, estimated from Mg, Si, Ca, Ti, is typical for objects of the thin disk (Reddy et al. 2003; 2006). Si and S abundances show moderate enhancements, i.e., $[Si/Fe] = +0.31$ and $[S/Fe] = +0.25$ respectively. The Zn abundance is derived from two lines at $\lambda 4722$ Å and $\lambda 4810$ Å. The value of $\log gf = -0.25$ for the line at $\lambda 4810$ Å was obtained from Barbuy et al. (2015). $[Zn/Fe] = -0.33$ is lower than expected for objects of the thin and thick disk population, i.e., ≈ -0.20 a -0.30 dex (Reddy et al. 2003; 2006). Neutron-capture elements show $[X/Fe]$ abundances with a tendency towards solar values and ranges from $+0.06$

TABLE 4
ELEMENTAL ABUNDANCES FOR HD 45674, HD 180028, HD 194951 AND HD 224893

Species	log ϵ_{\odot}	HD 45674			HD 180028			HD 194951			HD 224893		
		[X/H]	N	[X/Fe]	[X/H]	N	[X/Fe]	[X/H]	N	[X/Fe]	[X/H]	N	[X/Fe]
C I	8.39	-0.20±0.02	2	-0.36	-0.28±0.10	syn	-0.22	-0.16±0.09	5	-0.01	-0.11±0.10	2	+0.15
N I	7.78	+0.68±0.06	1	+0.52							+0.89±0.06	1	+1.15
O I	8.66	+0.03±0.01	2	-0.13	+0.07±0.10	syn	+0.13	-0.10±0.00	2	+0.05	+0.19±0.05	1	+0.45
Na I	6.17	+0.50±0.10	4	+0.34	+0.37±0.04	2	+0.43	+0.09±0.00	2	+0.24	+0.29±0.04	1	+0.55
Mg I	7.53	+0.08±0.19	4	-0.08	+0.19±0.09	1	+0.25	-0.21±0.09	5	-0.06	-0.34±0.11	3	-0.08
Si I	7.51				+0.19±0.14	3	+0.25	+0.18±0.06	2	+0.33			
Si II	7.51	+0.47±0.13	2	+0.31	+0.06±0.04	1	+0.12				-0.28±0.29	2	-0.02
S I	7.14	+0.41±0.10	5	+0.25	+0.38±0.09	3	+0.44	-0.03±0.10	syn	+0.12			
Ca I	6.31	+0.24±0.11	8	+0.08	+0.07±0.13	5	+0.13	-0.13±0.17	10	+0.02	-0.29±0.03	4	-0.03
Ca II	6.31	+0.16±0.15	2	0.00									
Sc II	3.05	+0.34±0.04	9	+0.18	+0.25±0.09	4	+0.31	-0.03±0.14	6	+0.12	+0.13±0.05	2	+0.39
Ti I	4.90	+0.27±0.10	3	+0.11	+0.15±0.06	1	+0.21	-0.21±0.06	2	-0.06			
Ti II	4.90	+0.29±0.14	14	+0.13	+0.05±0.10	4	+0.11	-0.18±0.12	13	-0.03	-0.20±0.11	13	+0.06
V II	4.00	+0.22±0.02	1	+0.06							-0.24±0.02	1	+0.02
Cr I	5.64	+0.13±0.08	3	-0.03	-0.11±0.10	2	-0.05	-0.34±0.13	5	-0.19	-0.25±0.12	2	+0.01
Cr II	5.64	+0.18±0.12	7	+0.02	-0.11±0.13	3	-0.07	-0.25±0.11	11	-0.10	-0.40±0.09	4	+0.14
Mn I	5.39	+0.14±0.01	3	-0.02	+0.11±0.08	4	+0.17	-0.21±0.18	5	-0.06	-0.21±0.03	1	+0.05
Fe I	7.45	+0.12±0.10	60		-0.06±0.13	56		-0.17±0.11	72		-0.27±0.11	19	
Fe II	7.45	+0.20±0.08	10		-0.06±0.16	8		-0.12±0.11	20		-0.26±0.17	7	
Ni I	6.23	-0.06±0.12	8	-0.22	-0.09±0.06	4	-0.03	+0.10±0.11	6	+0.25			
Ni II	6.23							+0.01±0.04	1	+0.16			
Cu I	4.21				-0.26±0.04	1	-0.20						
Zn I	4.60	-0.17±0.16	2	-0.33	-0.38±0.03	1	-0.32	-0.20±0.10	syn	-0.05	-0.26±0.03	1	0.00
Y II	2.21	+0.11±0.10	5	-0.05	+0.05±0.12	3	+0.11	-0.20±0.15	5	-0.05	-0.20±0.09	4	+0.06
Zr II	2.59	+0.61±0.13	3	+0.45	+0.10±0.04	1	+0.16	-0.12±0.19	2	+0.03			
Ba II	2.17	+0.35±0.07	1	+0.19	+0.23±0.10	syn	+0.29	-0.11±0.07	1	+0.04	-0.34±0.10	2	-0.08
La II	1.13				+0.29±0.05	1	+0.35						
Ce II	1.58	+0.33±0.14	3	+0.17	-0.08±0.16	3	-0.02						
Nd II	1.45	+0.22±0.05	1	+0.06	+0.13±0.09	2	+0.19	-0.11±0.17	2	+0.04			
Eu II	0.52				-0.12±0.10	syn	-0.06						

to +0.19 dex. Of other elements identified, like Y II, Ba II, Ce II and Nd II, only Zr II seems to be moderately enriched ($[Zr/Fe] = +0.45$).

5.2. HD 180028

HD 180028 was classified as a F6Ib and cataloged as an IRAS point source (IRAS 19122 + 0557). The radial velocity was reported by different authors: -6.0 km^{-1} (Wilson 1953), -6.0 km^{-1} (Dufflot et al. 1995) and -5.1 km^{-1} (Gontcharov 2006) and does not present variability. Its absorption lines appear slightly wide indicating that it rotates with a velocity of 23.3 km^{-1} (De Medeiros et al. 2002).

Their atmospheric parameters were obtained from ionization equilibrium between the lines of Fe I and Fe II, with values of $T_{\text{eff}} = 6400 \text{ K}$, $\log g = 2.1$, $\chi_t = 4.8$ and $[Fe/H] = -0.06$ dex respectively. The surface gravity for HD 180028 was confirmed from the equilibrium ionization of other elements such as Si, Ti, Cr, namely $\Delta = [X_{II}/H] - [X_I/H]$ is 0.11, -0.10

and -0.00 respectively. The atmospheric parameters obtained by different authors and the adopted parameters are displayed in Table 2.

HD 180028 exhibits a metallicity near to solar of $[Fe/H] = -0.06$. The abundance of C was obtained by synthesizing the line at 5380 \AA . We obtained values of $[C/H] = -0.28$ dex and $[C/Fe] = -0.22$ dex respectively. At a temperature of 6100 K the non-LTE correction to C was very small (Takeda 1994) and led to a value of $[C/Fe] = -0.39$ dex. There are no N lines or CN bands in the spectrum, so abundances could not be estimated. The O abundance was derived by synthesizing the region at $6140\text{--}60 \text{ \AA}$. The values are $[O/H] = +0.07$ dex and $[O/Fe] = +0.13$ dex, respectively (see Figure 3). These values are higher than those obtained by Luck (2014). The C/O ratio is about ≈ 0.23 , which is lower than the solar value. From a sodium analysis Andrievsky et al. (2002) found a moderate enrichment of $[Na/Fe] = +0.28$ dex. The value obtained in this work is slightly higher, i.e. $[Na/Fe] = +0.43$ dex. The Fe-peak elements show a solar trend. The ratio

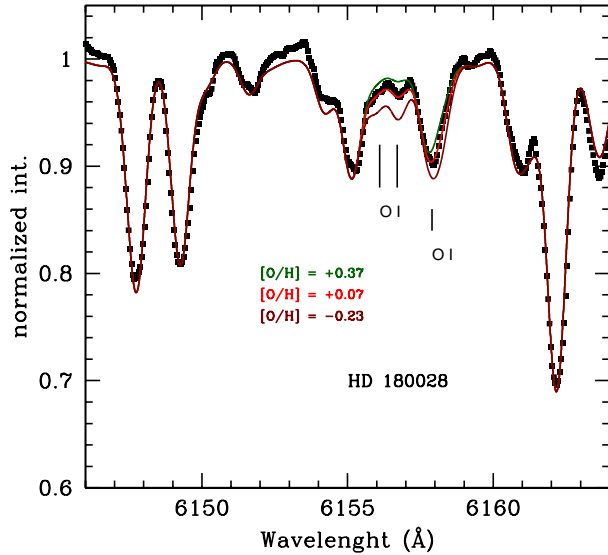


Fig. 3. Observed (filled squares) and synthetic (solid line) spectra of the OI triplet in the 6140–60 Å region. The synthetic spectra correspond from top to bottom to $[O/H] = +0.37$, $+0.07$ and -0.23 dex, respectively.

$[\alpha/Fe]$ of $+0.18 \pm 0.05$ dex seems to indicate that this object belongs to the thin disk. Individually, Si, Ca and Ti present solar values while Mg shows a moderate enhancement, $[Mg/Fe] = +0.25$ dex. Sulfur is found to be enriched, i.e., $[S/Fe] = +0.44$ dex. The s-elements show a solar trend except for Ba and La which are modestly enhanced.

5.3. HD 194951

HD 194951 was classified as F-type by different authors: F2Iab by Stock et al. (1960), F3II by Bidelman (1957) and F1III by Morgan (1972). The physical parameters have been determined by various authors using photometric and spectroscopic techniques (see Table 2). The values we adopted can be seen in Table 3. The surface gravity of HD 194951 was confirmed from the equilibrium ionization of other elements, such as Ti, Cr, and Ni, from which $\Delta = [X_{II}/H] - [X_I/H]$ is $+0.05$, $+0.09$ and -0.09 respectively. The chemical abundances of the elements identified are presented in Table 4.

The carbon abundance was determined from five lines ($\lambda 4769.9$ Å, $\lambda 4775.8$ Å, $\lambda 4932.0$ Å, $\lambda 5380.3$ Å and $\lambda 6014.8$ Å). We obtained a $[C/H]$ value of -0.16 . At a temperature of 7000 K the non-LTE effects were present and a correction of -0.2 dex for carbon led to values of $[C/H] = -0.36$ and $[C/Fe] = -0.26$ respectively. For the O abundance a non-LTE correction of -0.1 dex taken from Takeda & Takada-Hidai (1998) was estimated, and the abundances of

$[O/H] = -0.20$ and $[O/Fe] = -0.10$ are near to solar. These C and O abundance values are similar to those obtained by Luck (2014). The N line at $\lambda 4151.4$ Å found for HD 45674 and HD 224893 could not be measured. However, Lyubimkov et al. (2011) were able to study the N abundance for HD 194951 using high-resolution spectra and they found that N is enriched, with values of $[N/H] = +0.60$ and $[N/Fe] = +0.73 \pm 0.18$ respectively.

Our atmospheric model differs by 240 K and 0.12 in effective temperature and surface gravity relative to the model used by Lyubimkov et al., i.e., 6760 K and 1.92. In Table 3 we note that very few changes in the N abundance appear to be due to variations of 250 K and 0.5 in T_{eff} and $\log g$. This means that we can use this N abundance without being affected by the model. According to the authors the N enrichment is a general characteristic present in supergiant stars of A and F type that have experienced the first dredge-up (1DUP). The deficiency in C and the enrichment of N indicates that the CN-cycle has taken place and that processed material from the H-burning has been released on the surface of the star. The C/O = 0.46 ratio is practically solar, but it is an O-rich star.

The $[\alpha/Fe]$ ratio value of $+0.06$ is consistent for an object belonging to the thin disk population. The Si abundance exhibits a moderate enrichment, i.e., $[Si/Fe] = +0.33$. Other elements such as Sc, Cr, Mn and Zn show abundances $[X/Fe]$ between -0.15 and $+0.09$, similar to those present in objects of the thin and thick disk. The Zn abundance was obtained from the synthesized line at $\lambda 4810.5$ Å. $[X/Fe]$ of the s-elements ranges from -0.09 to $+0.01$, that is, it is on average solar.

5.4. HD 224893

Gray et al. (2001b) determined atmospheric parameters for this star (see Table 2) and it was classified as a bright giant, A8II. Several authors studied the radial velocity in different epochs, obtaining values (in km s^{-1}) of -22.4 (Adams 1915), -26.4 (Harper 1937), -23.2 (Wilson 1953), -21.9 (Bouigue et al. 1953), -27 (Fehrenbach et al. 1996) and -25.10 (Gontcharov 2006). These values show very little variation. Danziger & Faber (1972) report a rotation velocity of 40 km s^{-1} .

In this paper an analysis of abundances which includes a total of 15 elements was performed for the first time. The abundances are shown in Table 4. The metallicity of HD 224893 is moderately deficient ($[Fe/H] = -0.26$ dex). The C abundance

was obtained from the lines 4770.0 Å and 4771.7 Å respectively. From the LTE analysis we derived a value of [C/H] of -0.11 dex. By taking a non-LTE correction of -0.26 dex (Venn 1995b), both [C/H] and [C/Fe] reached values of -0.37 dex and -0.19 dex respectively. The N abundances obtained from $\lambda 4151.4$ Å were [N/H] = $+0.89$ dex and [N/Fe] = $+1.15$ dex respectively. The equivalent width of this line was 15.8 mÅ. With a non-LTE correction of -0.08 dex adopted at 7500K the new values were [N/H] = $+0.81$ dex and [N/Fe] = $+0.99$ dex respectively. Like HD 45674, this star shows evidence of having undergone the CN-cycle and the 1DUP event.

The O abundance is derived from the line at 6158 Å and shows signs of overabundance ([O/Fe] = $+0.45$). However, a non-LTE correction of -0.15 dex at a temperature of 7500K (from Takeda & Takada-Hidai 1998) leads to values of [O/H] = $+0.35$ dex and [O/Fe] = $+0.53$ dex respectively. These values indicate that the O abundance shows a moderate enrichment. The ratio C/O = 0.26 indicates that HD 224893 is O-rich and has a value similar to HD 45674.

The abundances [X/Fe] of the Fe-peak elements, such as V, Cr and Mn show solar values except Sc, which is moderately enriched by $+0.39$ dex. The alpha-elements ([α /Fe] = -0.02 dex); the Zn and the s-elements (Y and Ba) abundances resemble the solar values.

6. DISCUSSION

6.1. Atmospheric Parameters

The atmospheric parameters taken from the literature and those adopted in this work are present in Table 2. We take a mean value of atmospheric parameters of those objects with more than two values. We can note that our adopted values for the effective temperature, surface gravity, microturbulence velocity and metallicity are consistent (within the uncertainties) with the mean values derived by other authors.

6.2. Masses

We also estimated the masses of our sample stars. These can be obtained from their position on the HR-diagram using theoretical evolutionary tracks. We employed the theoretical evolutionary tracks without rotation for masses of 5, 7 and $9 M_{\odot}$, taken from Ekström et al. (2012) at solar metallicity ($Z=0.020$). Luminosities for HD 45674, HD 194951 and HD 224893

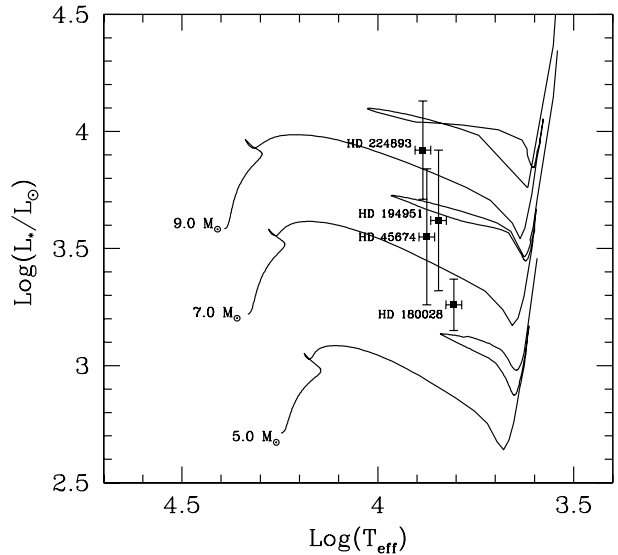


Fig. 4. Locations of HD 45675, HD 180028, HD 194951 and HD 224893 on the HR-diagram. The theoretical evolutionary tracks without rotation for masses of 5, 7 and $9 M_{\odot}$ are taken from Ekström et al. (2012) with $Z=0.020$.

were calculated using $M_V = V_0 + 5 - \log(D)$, where V_0 is the intrinsic colour derived from expression $V_0 = V - 3.1E(B - V)$ and D is the distance estimated from parallaxes (van Leeuwen 2007).

For HD 180028, however, the absolute magnitude was derived from a mean value ($M_V = -3.38 \pm 0.16$ mag) estimated by Kovtyukh et al. (2012). The bolometric corrections were taken from Masana et al. (2006) and we adopted a solar bolometric magnitude, $M_{\text{Bol}} = 4.73 \pm 0.01$ (Gray 2005).

The color excesses for HD 180028, HD 194951 and HD 224893 were obtained using $E(b - y)$ derived from Strömgren photometry by Gray et al. (2001b). We obtained $E(B - V)$ from the relation $E(b - y) = 0.78 E(B - V)$ (Fernie 1987). For HD 45674 the color excess was estimated from Schlafly's map (Schlafly & Finkbeiner 2011) where the dust in the Galactic disc was modelled assuming a thin exponential disc with a scale-height of 125 pc. A correction to the color excess ($B - V$) was applied with the last assumption. The values are listed in the eleventh column of Table 1.

Figure 4 shows the position of our sample stars on the HR-diagram. The uncertainty of the luminosities is based on the uncertainties of the parallaxes, visual magnitudes, extinctions and bolometric corrections. Individually, these uncertainties are 0.29 (HD 45674), 0.11 (HD 180028), 0.30 (HD 194951)

and 0.21 (HD 224893). According to their position we could estimate that HD 180028 has a mass of between 5 and 7 M_{\odot} , HD 45674 and HD 194951 between 7 and 7.5 M_{\odot} , and HD 224893 of about 9 M_{\odot} .

6.3. Evolutionary Status

CNO abundances are key to deduce the evolutionary status since their composition reflects the mixing process inside the stars. A summary is shown in Table 4. With respect to the light elements CNO, we note that the C abundances for HD 45674, HD 180028, HD 194951 and HD 224893 show deficiency with a non-LTE correction, i.e., they range from -0.04 to -0.69 dex.

Applying non-LTE corrections, HD 45674, HD 180028, HD 194951 and HD 224893 show values for the O abundance of -0.36 , $+0.02$, -0.10 and $+0.53$, respectively. HD 224893, by contrast, has a moderate enhancement ($[O/Fe] = +0.45$) probably due to the CNO bi-cycle. In general, our oxygen values show the observed tendency in objects of the disc studied by Bensby et al. (2014); da Silva et al. (2015).

For the total sample we were able to identify only one nitrogen line ($\lambda 4145.4 \text{ \AA}$) for HD 45674 and HD 224893. The values with NLTE corrections are $[N/Fe] = +0.36 \pm 0.11$ dex and $[N/Fe] = +0.99 \pm 0.14$ dex, respectively. Both objects show signs of CN processed material that has been brought to the surface. Since we were unable to estimate the abundance of nitrogen in HD 180028, we cannot argue about the efficiency of the CN-cycle. The N abundance in HD 194951 was previously studied by Lyubimkov et al. (2011), who found that nitrogen is enriched, i.e., $[N/Fe] = +0.73 \pm 0.18$ dex.

HD 45674, HD 194951 and HD 224893 show an enhancement of N abundance. These objects have shown a systematic deficiency of C and a systematic increase of N indicating the presence of CN-cycle material in the stellar surfaces. This enhancement of nitrogen was also reported by Venn (1995b), Venn & Przybilla (2003), Luck & Lambert (1985), Luck & Wepfer (1995) and Smiljanic et al. (2006) for supergiant and bright giant stars.

Three processes have been suggested to explain the surface nitrogen enhancement for massive stars. Each leads to the presence of CN-cycle material in stellar surfaces. In single stars these processes can be the severe mass loss, the rotationally induced mixing during the MS phase and the dredge-up associated with the deep convective envelope. According to Lyubimkov et al. (2011) the mass loss is unimportant for B-type stars (progenitors of A–F super-

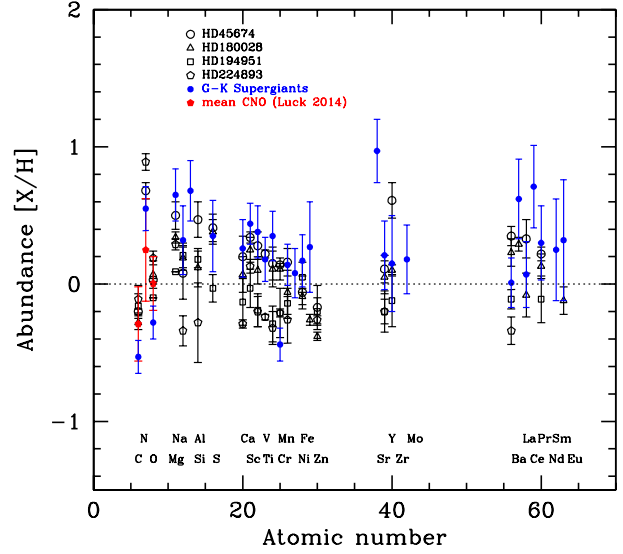


Fig. 5. Comparison of our abundances $[X/H]$ with the mean abundances for a sample of G–K young supergiants taken from Luck (1977; 1978) and mean CNO abundances by Luck (2014). Symbols and color represent data from different sources. The color figure can be viewed online.

giants) with masses ranging between 4–15 M_{\odot} . By contrast, the other two processes might be found coupled, e.g., it is an observational fact that the mixing process during the 1DUP event might differ between rotating and non-rotating stars. In binary stars, on the contrary, this enhancement can be due to mass transfer from an evolved companion.

In order to verify whether HD 45674, HD 194951 and HD 224893 have already passed through the 1DUP event is necessary to know the $[N/C]$ ratio. The post-1DUP prediction by Schaller et al. (1992) is approximately $[N/C] = +0.60$ dex for stars with masses between 2 and 15 M_{\odot} . On the other hand, Meynet & Maeder (2000) calculate rotating (with an initial velocity of 300 km s^{-1}) and non-rotating evolutionary models for masses between 9–120 M_{\odot} . These authors predict $[N/C] = +0.72$ dex without rotation and $[N/C] = +1.15$ dex with rotation after the 1DUP and during the blue loop phase for stars of 9 M_{\odot} . For more details see Figure 14 in Smiljanic et al. (2006).

For HD 194951, the $[N/C]$ ratio could be obtained from the N abundance derived by Lyubimkov et al. (2011) and the C abundance estimated in this work. Here, we must emphasize that our model differs by 240 K in T_{eff} and by 0.12 in $\log g$ from the model used by Lyubimkov et al. (2011). From

Table 3 we can see that there are small differences of -0.02 (in T_{eff}) and -0.06 (in $\log g$) respectively. These small differences do not affect the N abundance derived by Lyubimkov et al. (2011). Hence, it is possible to use the nitrogen abundance derived by Lyubimkov et al. (2011) with our C abundance. This value is $[\text{N}/\text{C}] = +0.81 \pm 0.17$ dex. For HD 45674 and HD 224893 we determined a $[\text{N}/\text{C}]$ ratio of $+0.88 \pm 0.09$ dex and $+1.00 \pm 0.13$ dex respectively. We note also that these values indicate that both stars show signs of an efficient mixing process. The mean $[\text{N}/\text{C}]$ ratio for the sample stars is $[\text{N}/\text{C}] = +0.90 \pm 0.13$ dex.

In short, our results for single and mean $[\text{N}/\text{C}]$ ratios are larger than the values obtained by Schaller et al. (1992) by a factor between 0.3-0.4 dex and are slightly above those of the non-rotating model of by Meynet & Maeder (2000), i.e., between $+0.72$ dex (non-rotating model) and $+1.15$ dex (rotating model). Our mean value $+0.90 \pm 0.10$ dex would be in agreement with the results for non-rotating stars with masses of $9 M_{\odot}$. Therefore, we may conclude that within the range of masses of our objects ($5-9 M_{\odot}$) and for their $[\text{N}/\text{C}]$ ratios, HD 45674, HD 194951 and HD 224893 have already experienced the 1DUP event and are in post-1DUP phase. Evolutionarily, the post-1DUP objects can be located only inside the red-blue loop area. Claret (2004) suggests that extensive red-blue loops occur for stars with masses from 6 to $13 M_{\odot}$, although this extension is still a matter of controversy (see § 6 and Figure 12 in Lyubimkov et al. 2011).

On the other hand, if we consider the effective temperature and luminosities to be right, HD 45674, HD 194951 and HD 224893 appear to be located within the extended red-blue region with $M = 7 - 9 M_{\odot}$ on the HR-diagram. However, the uncertainties cause an appreciable change in the luminosity so that their evolutionary status is unreliable. With regard to HD 180028, assuming a mass of $5 M_{\odot}$, its probable evolutionary status would place it in the red-blue loop region (post-1DUP phase). On the contrary, if we assume a mass of $7 M_{\odot}$ it would to be located on the Hertzsprung gap region and moving for the first time towards the red giant/supergiant phase (post-MS phase).

6.4. Sodium

In our sample we found a moderate enrichment of Na abundances, i.e., $[\text{Na}/\text{Fe}]$ of $+0.34$, $+0.43$, $+0.24$ and $+0.55$ for HD 45675, HD 180028, HD 194951 and HD 224893, respectively. It is believed that the sodium enrichment is related to the first dredge-up

event (Denissenkov & Denissenkova 1990) although this assumption is still debated. The predictions made by the models (see Fig. 8 in Karakas & Lattanzio 2014) indicate that sodium does not show a significant enrichment in low-mass stars ($M \leq 2 M_{\odot}$) from the first dredge-up or by extra-mixing process to solar metallicity (Charbonnel & Lagarde 2010). Even for $M > 2 M_{\odot}$ this enrichment does not exceed 0.3 dex.

A non-LTE correction of about of -0.10 dex to Na was taken from Lind et al. (2011) and results in values of $[\text{Na}/\text{Fe}]$ of $+0.16$, $+0.22$, $+0.24$ and $+0.37$ dex respectively. We note that our observational results (within their uncertainties) are in agreement with the $[\text{Na}/\text{Fe}]$ predicted by El Eid & Champagne (1995) for intermediate mass stars ($\approx 0.2-0.3$ dex).

6.5. Heavier Elements

The tendency shown by the alpha-elements of our objects is similar to that observed in the thin disk population, i.e., $[\alpha/\text{Fe}]$ ranges from -0.02 to 0.18 dex. The sulfur abundance was estimated synthesizing the spectral region at ($6743-6757 \text{ \AA}$). We obtained a $[\text{S}/\text{Fe}]$ of $+0.25$ for HD 45675 and $+0.12$ for HD 194951, showing a tendency similar to that observed for α -elements in the disc for metallicity near to solar value (Caffau et al. 2005). By contrast, S for HD 180028 is overabundant, i.e., $[\text{S}/\text{Fe}] = +0.44$ dex. Iron-peak and neutron-capture elements in all sample stars show $[\text{X}/\text{Fe}]$ abundances similar to the solar value. HD 45674 and HD 180028 show a modest enrichment of Zr II and La II of $+0.45$ dex and $+0.32$ dex, respectively.

6.6. Comparison With Other Supergiants

Our $[\text{X}/\text{H}]$ abundances can be compared with the mean abundances derived from a sample of G-K young supergiant stars studied by Luck (1977; 1978) and mean CNO abundances by Luck (2014). Figure 5 shows the $[\text{X}/\text{H}]$ abundances versus atomic number. The abundances in the sample stars of the present paper are shown with different symbols together with their uncertainties, namely HD 45674 (open circle), HD 180028 (open triangle), HD 194951 (open square) and HD 224893 (open pentagon). The cool supergiants are represented with a blue filled circle and CNO abundances with a red filled pentagon. We can see, in general, that abundances of our sample stars (e.g., CNO, α , Fe-peak and neutron capture elements) follow the trends expected from galactic chemical evolution for Population I stars.

7. CONCLUSIONS

We performed a detailed analysis of the photospheric abundances for a sample of four A–F type supergiant stars of intermediate mass ($\approx 5\text{--}9 M_{\odot}$) using high-resolution spectra. We determined atmospheric parameters, masses and abundances using spectral synthesis and equivalent widths. Three stars (HD 45674, HD 194951 and HD 224893), for which we were able to determine both carbon and nitrogen, show signs of internal mixing. A mean $[N/C]$ ratio of $+0.90 \pm 0.13$ dex was found; this value is in agreement with the predictions of non-rotating models by Meynet & Maeder (2000), which predict $[N/C] = +0.72$ dex. A surface nitrogen enhancement was observed in these stars and it can only be a result of deep mixing during the 1DUP. The sample of three stars shows very little variability in radial velocities, and hence binarity can be discarded.

According to the abundance analysis we can conclude that HD 45674, HD 194951 and HD 224893 have abundance values typical for supergiants of the thin disc population that have reached the post-first dredge-up (post-1DUP) phase. These objects are located in the red-blue loop region. HD 180028, on the contrary, shows abundances typical of Population I, but its evolutionary status could not be satisfactorily determined.

This work has made extensive use of ELODIE, SIMBAD and ADS-NASA databases for which we are thankful. The authors thank an anonymous referee for fruitful comments and suggestions that improved this work.

REFERENCES

- Adams, W. S. 1915, *ApJ*, 42, 172
 Andrievsky, S. M., Egorova, I. A., Korotin, S. A., & Burnage, R. 2002, *A&A*, 389, 519
 Asplund, M., Grevesse, N., & Sauval, A. J. 2005, *ASPC*, 336, 25
 Barbuy, B., Friaca, A.C.S., da Silveira, C. R., et al. 2015, *A&A*, 580, 40
 Bensby, T., Feltzing, S., & Oey, M. S. 2014, *A&A*, 562, 71
 Bidelman, W. P. 1957, *PASP*, 69, 326
 ———. 1993, *ASPC*, 45, 49
 Bouigue, R. & Chapuis, J. L. 1953, *PHOP*, 2, 50
 Caffau, E., Bonifacio, P., Faraggiana, R., Francois, P., Gratton, R. G., & Barbieri, M. 2005, *A&A*, 441, 533
 Castelli, F. & Kurucz, R. L. 2003, *IAUS, Modelling of Stellar Atmospheres*, ed. N. Piskunov, W. W. Weiss, & D. F. Gray (ASPC) A20
 Charbonnel, C. & Lagarde, N. 2010, *A&A*, 522, 10
 Claret, A. 2004, *A&A*, 424, 919
 Da Silva, R., Milone, A. C., & Rocha-Pinto, H. 2015, *A&A*, 580, 24
 Danziger, I. J. & Faber, S. M. 1972, *A&A*, 18, 428
 De Medeiros, J. R., Udry S., Burky G., & Mayor M. 2002, *A&A*, 395, 97
 Denissekov, P. A. & Denissenkova, S. N. 1990, *SvAL*, 16, 275
 Duflot, M., Figon, P., & Meyssonier, N. 1995, *BaltA*, 5, 83
 Ekström, S., Gorgy, C., Eggenberger, P., et al. 2012, *A&A*, 537, A146
 El Eid, M. F. & Champagne, A. E. 1995, *ApJ*, 451, 298
 Fehrenbach, C., Duflot, M., Genty, V., & Amieux, G. 1996, *BICDS*, 48, 11
 Fernie, J. D. 1987, *AJ*, 94, 1003
 Fürh, J. R. & Wiese, W. L. 2006, *JPCRD*, 35, 1669
 Gray, D. F. 2005, *The Observation and Analysis of Stellar Photospheres* (Cambridge: CUP), 506
 Gray, R. O., Graham, P. W., & Hoyt, S. R. 2001b, *AJ*, 121, 2159
 Gontcharov, G. A. 2006, *AstL*, 32, 759
 Harper, W. E. 1937, *PDAO*, 7, 1
 Hohle, M. M., Neuhäuser, R., & Schutz, B. F. 2010, *AN*, 331, 349
 Karakas, A. I. & Lattanzio, J. C. 2014, *PASA*, 31, 30
 Kaufer, A., Venn, K. A., Tolstoy, E., Pinte, C., & Kudritzki, R. P. 2004, *AJ*, 127, 2723
 Kurucz, R. L., Furenlid, I., Brault, J., & Testerman, L. 1984, *National Solar Observatory Atlas. National Solar Observatory, Sunspot, New Mexico*
 Kovtyukh, V. V. 2007, *MNRAS*, 378, 617
 Kovtyukh, V. V., Gorlova N. I., & Belik S. I. 2012, *MNRAS*, 423, 3268
 Lind, K., Asplund, M., Barklem, P. S., & Belyaev, A. K. 2011, *A&A*, 528, 103
 Luck, R. E. 1977, *ApJ*, 218, 752
 ———. 1978, *ApJ*, 219, 148
 ———. 2014, *AJ*, 147, 137
 Luck, R. E. & Lambert, D. L. 1985, *BAAS*, 17, 560
 ———. 1985, *ApJ*, 298, 782
 Luck, R. E., Moffett, T. J., Barnes III, T. G., & Gieren, W. 1998, *AJ*, 115, 605
 Luck, R. E. & Wepfer, G. G. 1995, *AJ*, 110, 2425
 Lyubimkov, L. S., Lambert, D. L., Korotin, S. A., Poklad, D. B., Rachkovskaya, T. M., & Rostopchin, S. I. 2011, *MNRAS*, 410, 1774
 Maeder, A., Meynet, G., Ekström, S., & Georgy, C. 2009, *PASA*, 26, 345
 Masana, E., Jordi, C., & Ribas, I. 2006, *A&A*, 450, 735
 Mélendez, J. & Barbuy, B. 2009, *A&A*, 497, 611
 Meynet, G. & Maeder, A. 2000, *A&A*, 361, 101
 Morgan, W. W. & Abt, H. A. 1972, *AJ*, 77, 35
 Moulataka, J., Ilovaisky, S. A., Prugniel, Ph., & Soubiran, C. 2001, *PASP*, 116, 693
 Prugniel, P. & Soubiran, C. 2001, *A&A*, 369, 1048
 Prugniel, P., Soubiran, C., Koleva, M., & Le Borgne, D. 2007, *ELODIE library V3.1, yCat: III/251*. Originally published in: *astro-ph/0703658*

- Przybilla, N. & Butler, K. 2001, *A&A*, 379, 955
- Reddy, B. E., Lambert, D. L., & Allende Prieto, C. 2006, *MNRAS*, 367, 1329
- Reddy, B. E., Tomkin, J., Lambert, D. L., & Allende Prieto, C. 2003, *MNRAS*, 340, 304
- Schaller, G., Schaerer, D., Meynet, G., & Maeder, M. 1992, *A&AS*, 96, 269
- Schlafly, E. F. & Finkbeiner, D. P. 2011, *ApJ*, 737, 103
- Smiljanic, R., Barbay, B., De Medeiros, J. R., & Maeder, A. 2006, *A&A*, 449, 655
- Snedden, C. 1973, PhD. Thesis, Austin-Texas, 180
- Soubiran, C., Le Campion, J. F., Cayrel de Strobel, G., & Caillo, A. 2010, *A&A*, 515, 111
- Stock, J., Nassau, J. J., & Stephenson, C. B. 1960, *LS*, 2, 0
- Stothers, R. B. & Chin, C. W. 1991, *ApJ*, 381, 67
- _____. 1976, *ApJ*, 204, 472
- Sumangala Rao, S., Giridhar, S., & Lambert, D. L. 2012, *MNRAS*, 419, 1254
- Takeda, Y. 1994, *PASJ*, 46, 53
- Takeda, Y. & Takada-Hidai, M. 1998, *PASJ*, 50, 629
- Van Leeuwen, F. 2007, *A&A*, 474, 653
- Venn, K. A. 1995a, *ApJS*, 99, 659
- _____. 1995b, *ApJ*, 449, 839
- Venn, K. A., Lennon, D. J., Kaufer, A., et al. 2001, *ApJ*, 547, 765
- Venn, K. A., Mc Carthy, J. K., Lennon, D. J., Przybilla, N., Kudritzki, R. P., & Lemke, M. 2000, *ApJ*, 541, 610
- Venn, K. A., Tolstoy, E., Kaufer, A. et al. 2003, *AJ*, 126, 1326
- Venn, K. A. & Przybilla, N. 2003, *ASPC* 304, *CNO in the Universe*, ed. C. Charbonnel, D. Schaerer, & G. Meynet (San Francisco, CA: ASPC) 20
- Walmswell, J. J., Tout, C. A., & Eldridge, J.,J. 2015, *MNRAS*, 447, 2951
- Wilson, R. E. 1953, *GCRV*, 601, 0
- Wu, Y., Singh, H. P., Prugniel, P., Gupta, R., & Koleva, M. 2011, *A&AS*, 525, 71

R. E. Molina: Laboratorio de Investigación en Física Aplicada y Computacional, Universidad Nacional Experimental del Táchira, Venezuela, (rmolina@unet.edu.ve).

H. Rivera: Laboratorio de Investigación en Física Aplicada y Computacional, Universidad Nacional Experimental del Táchira, Venezuela, (hrivera@unet.edu.ve).